Hindawi
Advances in Materials Science and Engineering
Volume 2018, Article ID 5014789, 10 pages
https://doi.org/10.1155/2018/5014789

Research Article

Study on Damping Energy Dissipation Characteristics of Cylindrical Metal Rubber in Nonforming Direction

Zhi Ying Ren[1,2] **Qisheng Chen**[1,2] **Hongbai Bai**[1,2] **and Yiwan Wu**[1,2]

[1]*Fuzhou University, School of Mechanical Engineering and Automation, Minhou Country Xueyuan Road No. 2, Fuzhou 350108, China*
[2]*Engineering Research Center for Metal Rubber, School of Mechanical Engineering and Automation, Fuzhou University, Fuzhou 350116, China*

Correspondence should be addressed to Hongbai Bai; bhb11.fzu@gmail.com

Received 23 July 2018; Accepted 9 October 2018; Published 5 November 2018

Academic Editor: Renal Backov

Metal rubber (MR) is an excellent damping material that is often used in practical engineering applications. The performance of MR in the nonforming direction is different from that in the molding direction, and research is rare; the anisotropy of MR is gradually revealed in many engineering applications because characterization and analysis of damping energy dissipation characteristics in the nonforming direction of cylindrical MR were carried out by the characterization method of damping materials. Based on the testing methods, dry friction and dynamic stiffness are taken as the main analysis points. By performing single-factor control and orthogonal tests, the parameters affecting the energy dissipation and damping characteristics of MR are studied, and the main factors that cause changes in energy consumption and loss factor are analyzed. It is found that the influence of loading amplitude on damping energy is much higher than that of loading frequency, and the damping characteristic of MR is not sensitive to frequency. Therefore, the loading amplitude level of the actual environment should be considered first followed by the knitting technology in design of MR components.

1. Introduction

"Metal rubber" (MR) possesses the same macromolecular structure and elasticity as rubber, although it is a metal product [1–3]. On the microcosmic point of view, the viscoelastic damping characteristics of the macroscopic MR are observed through the elastic deformation force of the spiral metal wire and the contact sliding interaction force between the spiral metal wires. Therefore, it has great advantages of high bearing capacity, fatigue resistance, no aging phenomenon, high temperature resistance, large temperature difference, radiation resistance, and corrosion environment [4, 5]. In special conditions, it shows obvious advantages such as improved life, reliability and performance of aerospace, naval equipment, and sophisticated military products [6–8]. Figure 1 shows the sample and the microstructure of the MR under electron microscope.

Therefore, MR has been studied intensively and attentively worldwide. At present, most of the studies are based on the mechanical properties and damping characteristics of the MR in the forming direction with few analyses in the nonforming direction. Taking the analysis of damping characteristics of the MR as an example, Hao et al. [9] carried out the dynamic tests on the biaxial compression MR isolator and concluded that the damping ratio of noncircular section wire MR is larger than that of ordinary MR. Li and Huang [10] changed the test weight and the height of the MR. The loss factor is obtained by the analysis and calculation of the MR isolator, which provides a certain basis for the dynamic response analysis of the MR. Wang et al. [11] analyzed the influence of acceleration on material damping characteristics by applying different acceleration loads to the MR shock absorbers. In terms of mechanical properties, many mechanical models of the forming direction, such as the pyramid model [12], laminated cantilever beam model [13], small curved beam model [14], microelement spring model [15], and porous material model [16], have been put forward.

(a) (b)

Figure 1: The sample (a) and microstructure (b) of the MR under electron microscope.

However, the working direction of many MR components used in the engineering application is their nonforming direction, such as the MR ring in the pipeline system [17] and MR block in the multidirectional vibration isolation [18]. In addition, similar applications exist in some similar damping material applications. Kwon et al. proposed a novel pseudoelastic gear that utilized the ring-type SMA mesh washer as a spring blade to bridge the output shaft of the motor with an existing gear wheel [19], and Oh et al. proposed a whole antenna isolation system employing a ring-type SMA mesh washer that supports the gimbal-type antenna [20].

Besides, our group previously found that the elastic damping characteristic of a nonforming direction MR is obviously different from that of the forming direction MR [21]. Figure 2 represents the hysteresis recovery force curve of MR at different directions. It can be seen that the average stiffness of the nonforming direction is obviously greater than that of the forming direction, which indicates that MR is an anisotropic material.

Therefore, it is necessary to further study the damping energy dissipation characteristics of an MR in the nonforming direction. However, works on the performance of the nonforming direction (nonbearing direction) are not comprehensive enough. Rua et al. [22] calculated the basic parameters of an MR material using experimental data and then simulated its performance using the finite element method. The results showed that the simulation method has a high solution precision and is suitable for the static mechanical calculation. Wu et al. [23] compared the radial force on the MR parameters with some of the MR parameters such as weight, density, and temperature. The mechanical model of MR is established, which can comprehensibly describe the load-deformation relationship of MR.

However, these studies are based on statics, and there is almost no study on the dynamic damping energy dissipation characteristics of MR in the nonforming direction. Therefore, in this paper, the damping characteristic of a cylindrical MR in the nonforming direction is characterized. The engineering significance of different parameters of the studied MR, such as the knitting mode, the density, the test amplitude, and the test frequency, is also emphasized.

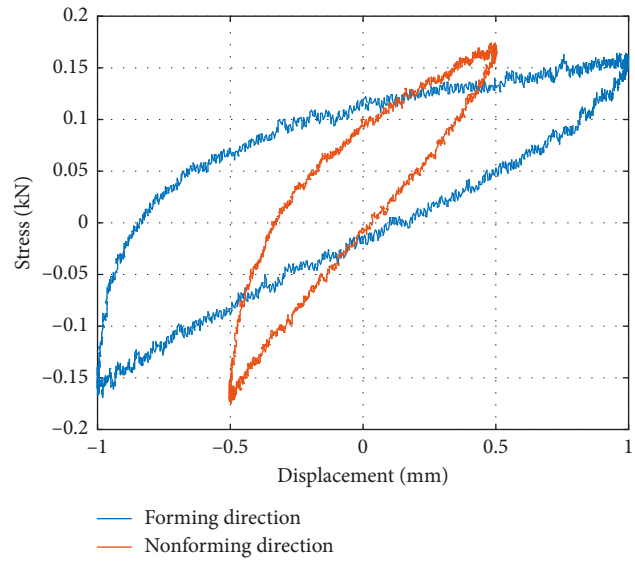

Figure 2: Hysteresis loop of MR in the forming/nonforming direction.

2. Compression Characteristics and Deformation Mechanism of MR

The studied MR is made of a stainless steel wire that is only 0.1–0.4 mm in diameter produced through the process of wire selection, wires winding, stretching, blank weaving, molding, cleaning, and so on. Figure 3 displays a roughcast of the MR wrapped around and the molding diagram of the MR. The loading and unloading tests are carried out; thus, the hysteresis recovery force curve of the MR in different directions is obtained, as shown in Figure 4.

This property of MR is related to the spatial distribution and orientation of internal metal spiral coils of MR. After the MR is formed, the relative position between the spiral rolls is not completely random, and the plane of most spiral rolls is parallel to the normal plane in the direction of the pressure formed. When the MR bears load, the spiral coil is extruded and deformed, with increasing deformation, the contact between the spiral rolls will slip, and the sliding contact points are restricted by the change in the geometric position of the spiral coil and the restriction of the other spiral rolls.

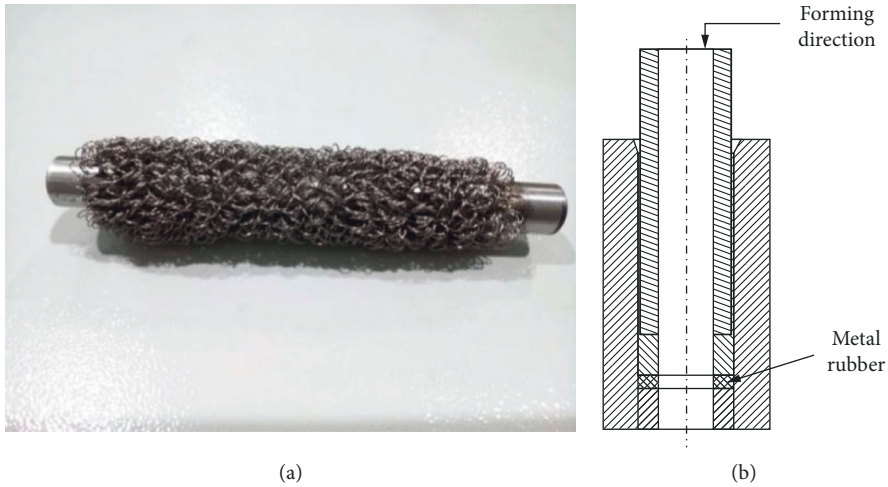

Figure 3: A roughcast of MR wrapped around (a) and the molding diagram of the MR (b).

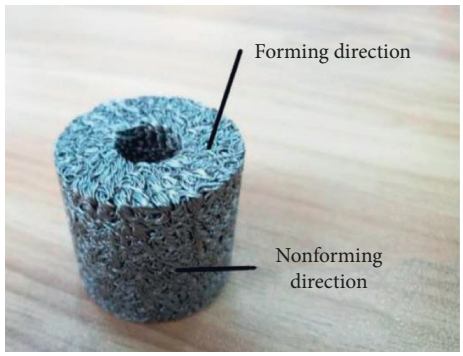

Figure 4: Different forming directions of MR.

The spiral rolls are divided into multiple sections of curved beams at the contact point. These curved beams are interlaced and interlocked together. The elastic damping property of MR is mainly formed by the elastic deformation force of curved beams and the interaction between curved beams.

In the nonforming direction, the deformation of the curved beam is not the compression deformation in the forming direction but the deformation of the spiral wire itself. Because the stiffness of the curved beam in the nonforming direction is generally greater than that in the forming direction, the average stiffness of the MR in the nonforming direction is greater than that in the forming direction.

At present, more and more nonforming directions of the MR have been applied in the field of engineering. However, researchers mainly studied the mechanical properties of MR in the forming direction, while a little has been done on the mechanical properties in the nonforming direction. Therefore, in this study, the relationship between the parameters of the MR that affect the nonforming direction properties is obtained, analyzing the stiffness parameters. Finally, the structural design of MR which guides the nonforming direction is realized, and the energy dissipation performance in the nonforming direction of MR has also been improved.

3. Damping Parameters and Testing Method of the MR Material in Nonforming Direction

3.1. Damping Parameters Characterization. Damping materials are designed to reduce the impact of large vibration on operation accuracy and stability. It mainly decreases the magnitude of vibration by transforming the vibration energy of external excitation into other forms of energy. There are many parameters to characterize the damping properties of materials. The most commonly used measurement parameters are the damping ratio, the phase difference angle tangent, the loss factor, the logarithmic attenuation rate, and the reciprocal of the quality factor. Due to the nonlinear characteristics of the material, some testing methods based on the linear principle cannot be used; thus, the loss factor is used as the damping characterization of the MR material in this study [24].

3.2. Calculation Method of Damping Test Parameters for the MR Material. In order to measure the loss factor, the sinusoidal excitation method is used to collect and calculate the damping material of the MR. The sinusoidal excitation method is directly used to calculate the energy dissipation and maximum elastic potential energy in a period using an electrohydraulic servo material tester. Then, the MR element restoring force response signal is measured applying the sinusoidal displacement load to the MR material. In this experiment, an SDS-200 high- and low-temperature dynamic and static material testing machine (Figure 5) was used to load the MR under sinusoidal force, and thereafter, the response was collected. The maximum working load of the tester was 200 kN, and the test frequency was 0.01–40 Hz.

The sinusoidal alternating displacement in the following equation is applied to the tested parts using the servo-controlled material testing machine:

$$X = X_0 \cos(\omega t + \alpha), \tag{1}$$

where α is the initial phase, X_0 is the amplitude of the test input, and ω is the loading cycle.

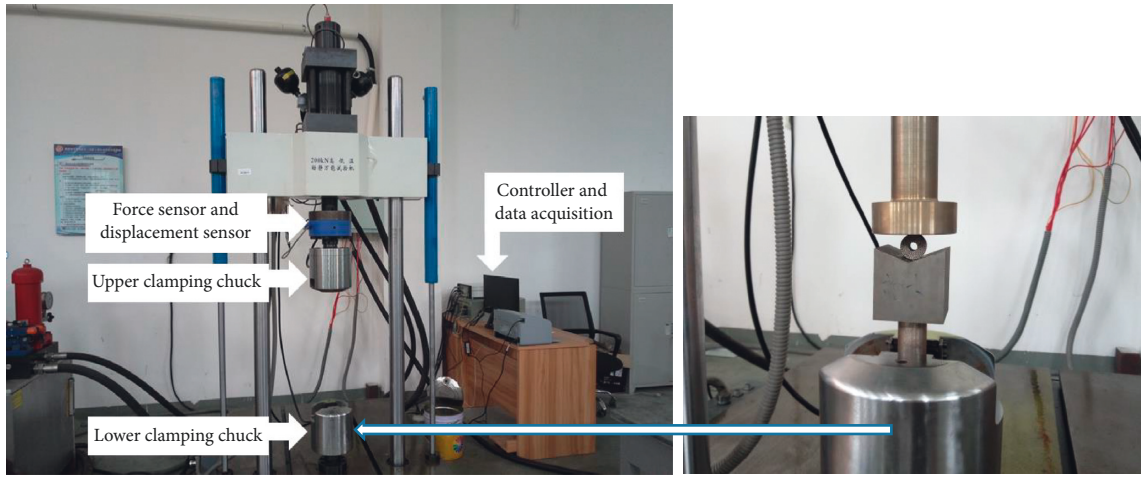

(a) (b)

Figure 5: Dynamic (a) and static (b) material testing machine used in the present study.

The energy consumed by an MR specimen in one cycle is ΔW, that is, the area surrounded by a hysteresis loop:

$$\begin{aligned}\Delta W &= \oint F\,dx,\\ \Delta W &= \oint Fd\left[X_0\cos\left(\omega t+\alpha\right)\right],\\ \Delta W &= -\omega X_0\int_0^T F\sin\left(\omega t+\alpha\right)(t).\end{aligned} \tag{2}$$

According to the experimental conditions, the integral formula in Equation (2) is discretized and then the new formula is obtained [25]:

$$\begin{aligned}\Delta W &= -\frac{2\pi X_0}{N}\sum_{i=1}^{N}F_i\sin\left(\frac{2\pi i}{N}+\alpha\right),\\ N &= \frac{f_0}{f},\end{aligned} \tag{3}$$

where N is the number of discrete points in a cycle; f_0 is the sampling frequency for the system, $f_0 = 2500$ Hz; and f is the loading frequency.

In order to calculate the maximum elastic potential energy storage of materials, the dynamic average stiffness K is defined using the following equation:

$$K = \frac{F_{\max}-F_{\min}}{2X_0}. \tag{4}$$

Therefore, the maximum elastic potential energy stored in the material W would be

$$W = \frac{1}{2}\overline{K}X_0^2 = \frac{\left(F_{\max}-F_{\min}\right)}{2}X_0, \tag{5}$$

where $F_{\max}$ and $F_{\min}$ are the maximum and minimum values of restoring force collected in the sampling system, respectively.

The loss factor η is the ratio between the loss energy and the maximum elastic energy in the system, and the loss factor can be calculated using Equations (3) and (5). In general, the larger the loss factor is, the better the damping performance is:

$$\eta = \frac{\Delta W}{2\pi W} = -\frac{4f}{f_0\left(F_{\max}-F_{\min}\right)}\sum_{i=1}^{N}F_i\sin\left(\frac{2\pi i}{N}+\alpha\right). \tag{6}$$

4. Experimental Design and Result Analysis

4.1. Loading Pretest. Plastic deformation may occur when the metal material is subjected to excessive load [26], and the memory alloy is very useful to overcome the plastic deformation problem of metal materials [27]. Therefore, in this paper, the scope of loading capacity of MR is obtained by the pretest method, and the force loading test of MR with different densities is carried out. The experimental results are shown in Figure 6. From the graph, the force loading curves of MR with different densities are almost linear; that is, the MR materials satisfy the generalized Hooke's law. It is indicated that MR exhibits linear elasticity within a certain load range. At the load level of 1 kN, the load-displacement curve of MR does not change; that is, there is no plastic deformation [28]. Therefore, we can ensure that the plastic deformation does not become a variable affecting the test accuracy through this preliminary experiment.

4.2. Experimental Design. The tooling is sandwiched between upper and lower heads of the material test machine, the cylindrical MR specimen is put into the clamp, and the clamp is trimmed on it, so as to prevent the loading process from breaking out of the tooling. The pretightening amount is represented by the displacement of the beam, X_a:

$$X_a = 2X_0, \tag{7}$$

where X_0 is the amplitude. The position after pretightening is assumed as the equilibrium position of sinusoidal displacement loading, and sinusoidal excitation is applied to the specimen (displacement control). The force-displacement

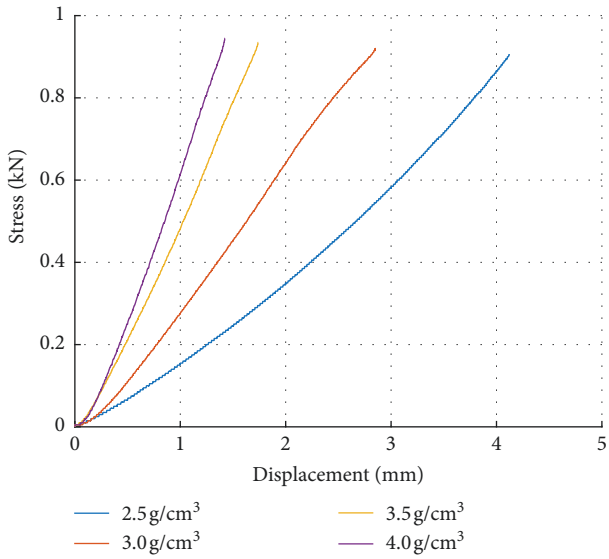

Figure 6: Force loading tests of MR with different densities.

signal is sampled by means of a data acquisition device, at the frequency f_0 of 2500 Hz.

In order to investigate the influence of different parameters on the damping property of MR and the degree of influence of various parameters, the experiment is divided into two parts. The first part comprised a single-factor controlled trial. The effect of single factor on the damping characteristic of the nonformed direction MR is compared to the results of the test. The second part comprised the orthogonal test using various factors, and the degree of interaction between the parameters was obtained by range analysis.

4.3. Influence of Single Factor on Damping Characteristics of MR in Nonforming Direction. The characterization parameters of MR specimens are shown in Table 1. The size of the specimen is $D30 \times d10 \times h30 \pm 1$ mm. As shown in Figure 7, the density of MR specimens is 2.5 and 3.5 g·cm^{-3}.

4.3.1. Influence of Different Loading Frequencies on Energy Dissipation Characteristics. Figures 8 and 9 are the dynamic hysteresis loops in the nonforming direction, respectively, which are realized by different densities of MR under different loading frequencies.

From the diagram, it is evident that the hysteresis loop shape of the MRs obtained after the sine excitation loading test shows a sickle type. Due to the nonlinear characteristics of MR materials, the pores between metal wires are filled during loading, and the friction between wires begins to rub. Both dynamic average stiffness and energy consumption increase gradually. In addition, the left half area of the hysteresis loop in the diagram is larger than the right half area of the $y = 0$ axis, which means that the energy consumption of the compressed part is greater than that of the restorer in the loading process (i.e., compression process).

The hysteresis loop diagram shows that the hysteresis loop of MR formed by different loading frequencies is mostly in the state of reclosing. It indicates that the energy dissipation of MR components at different frequencies and in the same amplitude is approximately the same. It is shown that the damping performance of MR components is not significantly affected by different excitation; in other words, the damper prepared by MR has good stable damping performance. It can be found that the restoring force of the lower density specimen decreases with increasing loading frequency, and the hysteresis loop has a relatively large fluctuation (Figures 8 and 9). When the density is higher, the restoring force increases with the increase of loading frequency, and the hysteresis loop is found to be smooth relatively. The reason for this phenomenon is as follows: when the density is relatively small, the gap between the metal wires is relatively large, and the slip distance between the wires is larger. Then, the dry friction between the wires is changed from static friction to dynamic friction, which will form a big jump in the curve.

Table 1: Single-factor control test of MR test parameters.

Number	Frequency (Hz)	Density (g·cm^{-3})	Amplitude (mm)	d (mm)	Methods
1	1, 2, 3, and 4	2.5 and 3.5	0.5	0.15	Twining
2	1	2.5, 3.0, 3.2, and 3.5	0.5	0.15	Twining
3	1	2.5	0.5, 0.8, 1.0, and 1.2	0.15	Twining
4	1	2.5	0.5	0.15 and 0.3	Netting and twining

The actual change in the material is difficult to obtain from the hysteresis loop, so the loss factor, energy consumption, and dynamic average stiffness calculated by the MATLAB program are listed in Table 2. And the change law is shown in Figure 10.

Comparing the changes in the parameters of MR components with two different densities under the sinusoidal excitation, it is found that the low-density MR has larger porosity, and the pores are filled first under the condition of low loading amplitude. However, the energy consumption changes little with density as the energy consumption is the elastic energy of the metal wire bending which does not change with density. In addition, the wire did not return to the original space pore in the process of returning, which will lead to a decrease in dynamic average stiffness and maximum elastic potential energy and a small increase in loss factor. While the high-density MR itself has a small pore space, the friction energy between the wires is completed during the loading process. Under the continuous loading, the friction is more intense. Therefore, both energy consumption and the dynamic average stiffness show a rising trend. And the loss factor has a very small downward trend.

4.3.2. Influence of Structure Density on Energy Dissipation Characteristics. In order to find the effect of density on energy consumption of materials, four groups of specimens with a density of 2.5, 3, 3.2, and 3.5 g·cm^{-3} were designed. As

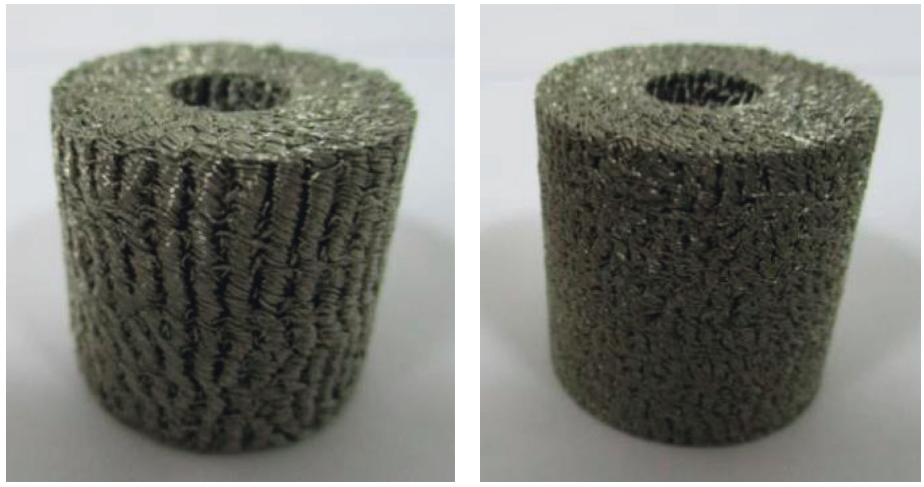

(a) (b)

Figure 7: MR specimen with different densities. (a) $\rho_{MR} = 2.5\,g{\cdot}cm^{-3}$. (b) $\rho_{MR} = 3.5\,g{\cdot}cm^{-3}$.

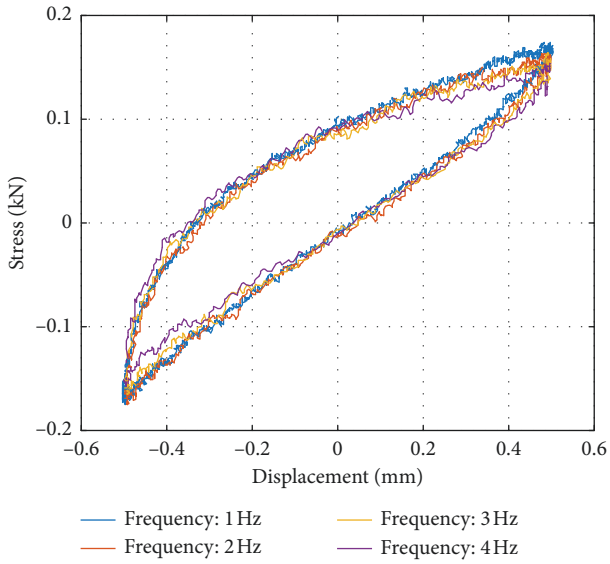

Figure 8: Dynamic hysteresis loop of MR with the density of $2.5\,g{\cdot}cm^{-3}$ under different loading frequencies.

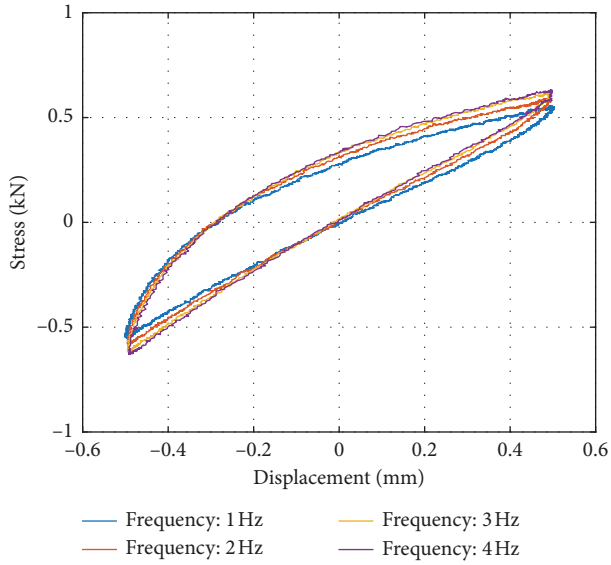

Figure 9: Dynamic hysteresis loop of MR with the density of $3.5\,g{\cdot}cm^{-3}$ under different loading frequencies.

shown in Figure 11, the hysteresis characteristics of the MR with different densities are different, and the graphic area increases by increasing the density of the specimen. Therefore, with higher density, the stronger energy dissipation capacity of the MR is obtained. However, the change in loss factor shows an opposite character because the loss factor is affected by maximum elastic energy storage, and the maximum energy storage is related to the stiffness (Figure 12). The maximum energy storage increases with stiffness. The dynamic stiffness of MR increases with the increase of density, while the decrease rate of loss factor increases with the increase of stiffness. Therefore, the energy dissipation characteristics of MR are highly correlated with materials density; i.e., MR elements with low density possess better damping characteristics.

Table 2: Loss factor, energy dissipation, and dynamic average stiffness variation.

f (Hz)	1	2	3	4
$\eta_{\rho_{MR}2.5}$	0.3461	0.3311	0.3224	0.3171
$\Delta W_{\rho_{MR}2.5}$	0.0837	0.0817	0.0808	0.0812
$K_{\rho_{MR}2.5}$	0.32	0.32	0.31	0.29
$\eta_{\rho_{MR}3.5}$	0.2693	0.2670	0.2640	0.2629
$\Delta W_{\rho_{MR}3.5}$	0.2251	0.2402	0.2521	0.2583
$K_{\rho_{MR}3.5}$	1.12	1.16	1.17	1.21

4.3.3. Influence of Different Amplitudes on Energy Dissipation Characteristics. The influence of different amplitudes on the energy dissipation characteristics of MR was examined by maintaining the pretightening amount, where the maximum amplitude of 1.2 mm is selected for this study. The same sine

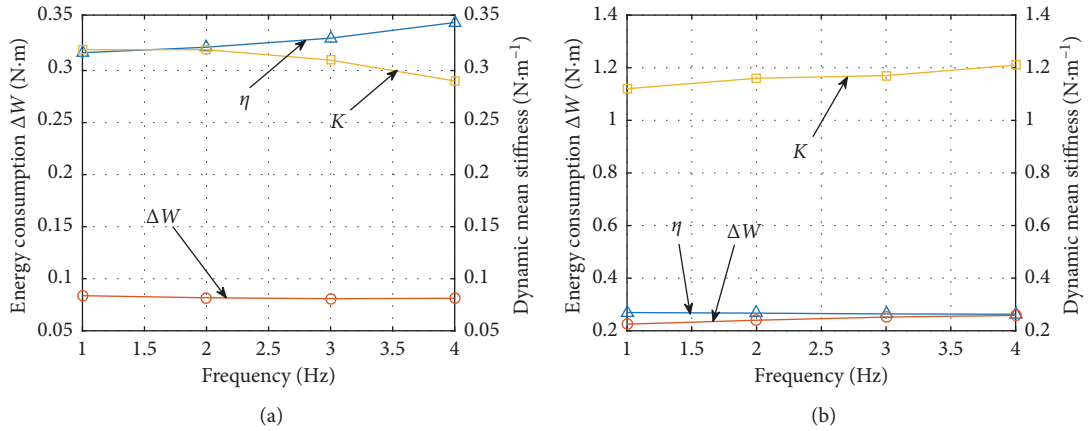

Figure 10: The loss factor, energy dissipation, and dynamic average stiffness variation at different frequencies. (a) MR with the density of 2.5 g·cm^{-3}. (b) MR with the density of 3.5 g·cm^{-3}. η is the dissipation factor.

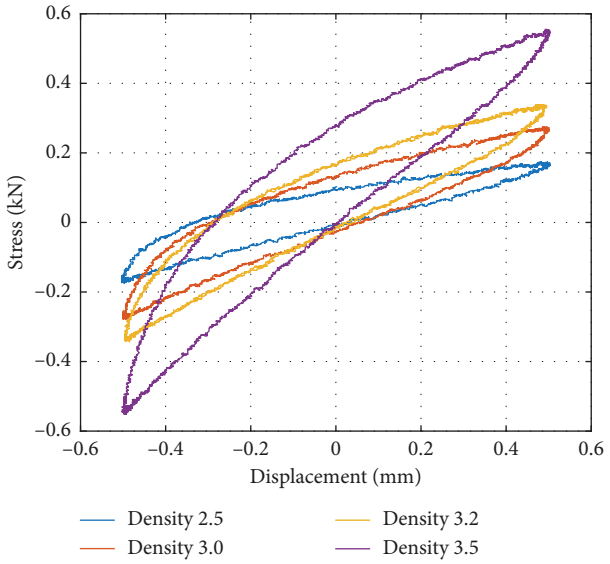

Figure 11: Hysteresis curve of MR with different densities.

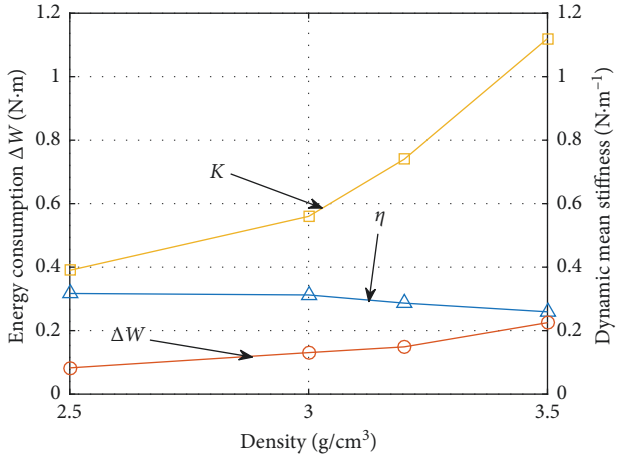

Figure 12: Loss factor and dynamic average stiffness K with changing density. η is the dissipation factor.

excitation origin for all four sets of data is ensured so that the test comparison becomes more accurate. The hysteresis loop of MR in very forming direction is shown in Figure 13. The change in loss factor, energy consumption, and average dynamic stiffness under the effect of different amplitudes is shown in Table 3, and the trend of change is shown in Figure 14.

From the graph, it is evident that the area surrounded by hysteresis loops increases with the increasing amplitude, meaning that the energy loss increases. In addition, with the increase of amplitude, the value of the maximum elastic potential energy increases. Simultaneously, a downward trend in loss factor and stiffness is found (Figure 14).

This phenomenon is because when the amplitude increases at a certain frequency, the compression degree of the MR increases and the number of contact points of the wire increases. However, in the course of returning, the wires are still in contact with each other because of the strong elastic properties of the wire so that the return speed is slower than that of the external load. The energy dissipation effect has a downward trend.

4.3.4. Influence of Different Braiding Process Parameters on Energy Dissipation Characteristics. Figure 15 shows three kinds of specimens with different knitting processes to study the influence of different knitting processes on the energy dissipation characteristics of MR. Then, the sinusoidal excitation of MR with different process parameters was carried out to obtain the hysteresis loop (Figure 16), and the variation of the parameters on the hysteresis loop is also investigated (Figure 17). The summary of loss factor, energy dissipation, and dynamic stiffness is listed in Table 4.

A progressive relationship between the energy dissipation capacities of MR under the three process parameters, which is due to the increase of stiffness, is visible (Table 4). Therefore, according to the knitting process, with a larger wire diameter, the wire stiffness is higher that causes higher energy consumption. The netting MR has more contacts in the mesoscopic structure than the twisted MR,

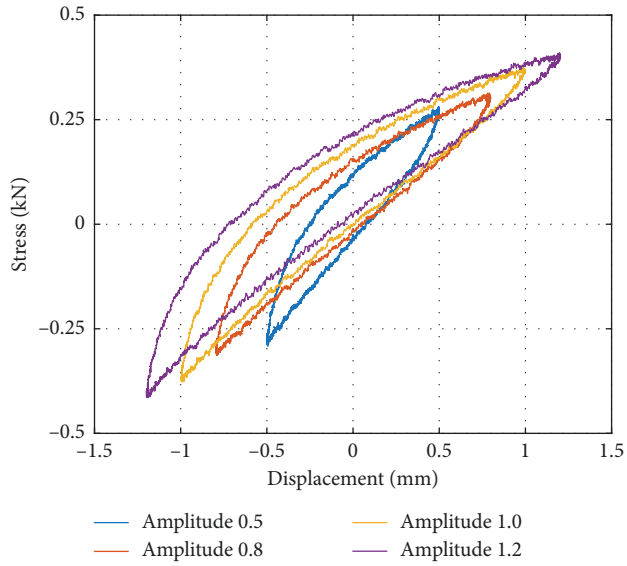

Figure 13: Hysteresis loops of MR under different amplitude conditions.

Table 3: Loss factor, energy dissipation, and dynamic average stiffness variation.

Amplitude (mm)	0.5	0.8	1.0	1.2
η	0.2881	0.2832	0.2658	0.2449
ΔW	0.1238	0.2146	0.3033	0.3700
K	0.52	0.44	0.37	0.33

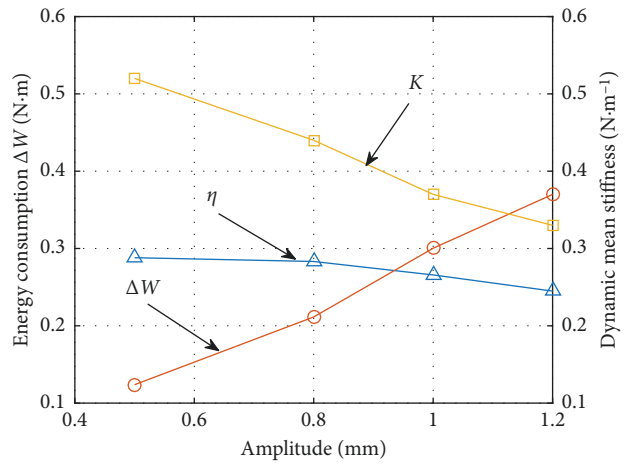

Figure 14: The variation curves of each parameter under different amplitudes. η is the dissipation factor.

and the structure is more stable. The dry friction energy consumption of the netting MR sample is much earlier than that of the twisted MR sample, so that the rigidity is greater and thus the energy consumption is greater. From the abovementioned analysis, it is obvious that loss factor of the braided MR is more affected by the stiffness, giving a decreasing trend.

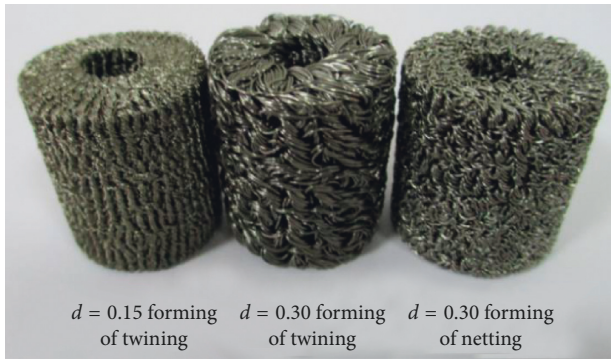

Figure 15: MR with different weaving process parameters.

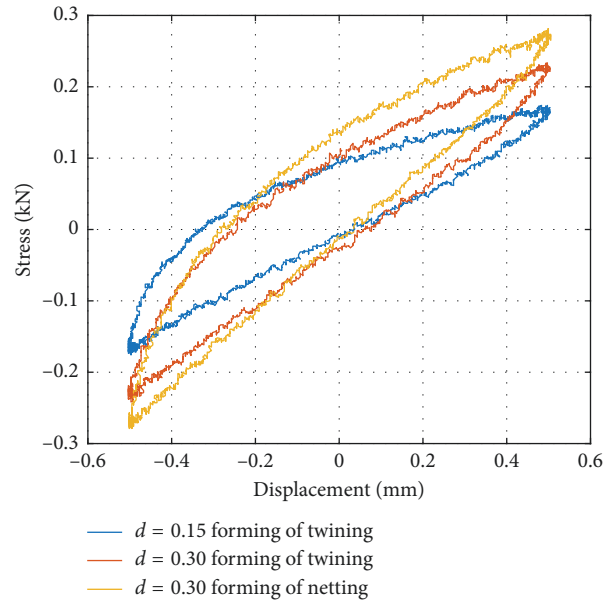

Figure 16: Hysteresis loop of MR under different processes.

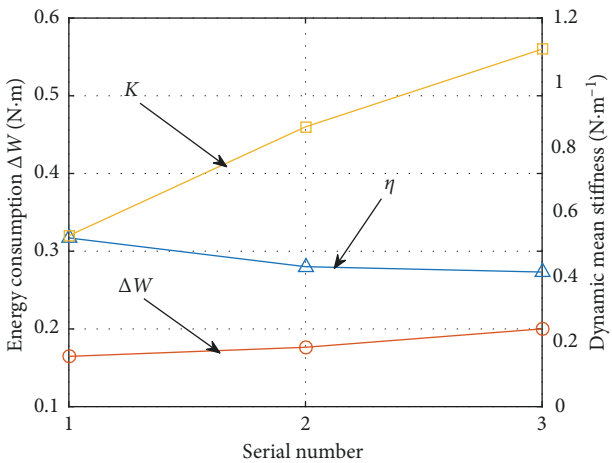

Figure 17: Parameter variation curves under different processes. η is the dissipation factor.

4.4. Orthogonal Test and Result Analysis of Various Parameters. The above experiment is based on control variables and explains the influence of various factors on the

Table 4: Loss factor, energy dissipation, and average dynamic stiffness.

Serial number	1	2	3
Methods	d = 0.15 and twining	d = 0.30 and twining	d = 0.30 and netting
η	0.3461	0.2801	0.2732
ΔW	0.1647	0.1764	0.2001
K	0.32	0.46	0.56

damping energy consumption of MR from the viewpoint of dry friction. In order to investigate the sensitivity of various factors to damping energy consumption, an orthogonal test was designed. According to the influence of the damping property parameters of MR, four test factors such as density (A), amplitude (B), test frequency (C), and molding process (D) have been selected. Each factor has 3 levels. Specific factors and factors level selected are shown in Table 5. The loss factor is used as the experimental index. Therefore, we chose orthogonal arrays to carry out 9 orthogonal experiments. The specific factors are shown in Table 6.

As shown in Table 6, under different parameter levels, by increasing the loss factor, better damping performance is obtained. By comparing the extreme values at the level of each parameter, primary and secondary relationships of different factors (B > D > A >C) can be obtained, which means amplitude > forming condition > density > frequency.

It can be seen that the effect of amplitude on the loss factor is most obvious, while the frequency is less affected. The difference between density and molding conditions is close, both of which are design parameters, and their effect on stiffness is obvious.

5. Conclusion

(1) According to the single-factor control test results, with the increase of dynamic stiffness, the level of energy consumption is significantly improved. The low-density MR energy dissipation is achieved by overcoming the bending of the steel wire, so it loses less energy. By increasing the density of MR, the main form of energy dissipation changes to the friction between the wires, which causes the energy consumption rate to increase rapidly. At different loading frequencies, the motion of the metal wire only changes with speed, which has little effect on stiffness and a small change in dissipative energy. The damping property of MR is characterized by loss factor. The loss factor is proportional to energy consumption and affected by the maximum elastic energy storage.

(2) The influence of different factors on the damping property is studied by performing the orthogonal test. The order of the factors that affect the damping performance is found to be amplitude > molding condition > density > frequency. The result shows that the effect of amplitude on damping energy is much greater than that of frequency in practical application, so the damping characteristic of the MR element is not sensitive to loading frequency. Therefore, when the MR components are designed, the amplitude level of the actual environment should be considered first followed by a suitable technology.

Table 5: Orthogonal test factors and their level.

Factor	Symbol	Levels		
		1	2	3
Density	A	2.5	3.0	3.5
Amplitude	B	0.5	0.8	1.0
Frequency	C	1	3	5
Condition of molding	D	0.15 forming of twining	0.3 forming of twining	0.3 forming of netting

Table 6: Orthogonal test results of the loss factor index.

	Density	Amplitude	Frequency	Condition of molding	Loss factor
	A	B	C	D	
1	1	1	1	1	0.3461
2	1	2	2	2	0.2979
3	1	3	3	3	0.2366
4	2	1	2	3	0.2669
5	2	2	3	1	0.2795
6	2	3	1	2	0.1999
7	3	1	3	2	0.2843
8	3	2	1	3	0.2476
9	3	3	2	1	0.2670
$K1$	0.8806	0.8973	0.7936	0.8926	
$K2$	0.7463	0.8250	0.8318	0.7821	B > D > A >C
$K3$	0.7989	0.7035	0.8004	0.7511	
Extreme difference	0.1343	0.1938	0.0382	0.1415	
Rank	3	1	4	2	

Data Availability

The data used to support the findings of this study are available from the corresponding author upon request.

Conflicts of Interest

The authors declare that they have no conflicts of interest.

Acknowledgments

We thank the National Natural Science Foundation of China (Grant no. 51805086), Fujian Provincial Natural Science Foundation (2015J01195), High-end Bearing Tribology Technology and Application, National Joint Engineering Laboratory Open Fund Project, and Henan University of Science and Technology (201802).

References

[1] Z. Y. Li and Z. R. Lu, "Research on combined stiffness characteristic of metal rubber damper," *Journal of Harbin Institute of Technology*, vol. 37, no. 11, pp. 1294–1297, 2005.

[2] Y. Q. Chen, B. T. Guo, and Z. G. Zhu, "The investigation of the stiffness characteristics and the stress-strain relation of metal rubber," *Journal of Aerospace Power*, vol. 17, no. 4, pp. 416–419, 2002.

[3] H. Y. Jiang, H. Yan, and H. R. Ao, "Calculation of elastic damping characteristics of rotor support made of metal rubber material under variable load," *Chinese Journal of Mechanical Engineering*, vol. 20, no. 6, pp. 33–37, 2007.

[4] H. Zuo, Y. H. Chen, and H. B. Bai, "The compression deformation mechanism of a metallic rubber," *International Journal of Mechanics and Materials in Design*, vol. 2, no. 3-4, pp. 269–277, 2005.

[5] J. F. Hou, H. B. Bai, and D. W. Li, "Experimental investigation on fatigue characteristics of metal-rubber matierial at high and low temperature," *Aerospace Material and Technology*, no. 2, pp. 77–80, 2007.

[6] Y. H. Ma, X. L. Tong, B. Zhu, D. Y. Zhang, and J. Hong, "Theoretical and Experimental Research on thermal physical properties of metal rubber," *Journal of Physics*, vol. 62, no. 4, pp. 470–479, 2013.

[7] Z. Lin, G. Z. Li, H. B. Bai, and C. H. Lu, "Research progress of corrosion test methods for metallic materials in marine environment," *New technology and Pro Expansion*, no. 8, pp. 68–74, 2013.

[8] B. Zhang, Z. Q. Lang, S. A. Billings, G. R. Tomlinson, and J. A. Rongong, "System identification methods for metal rubber devices," *Mechanical Systems and Signal Processing*, vol. 39, no. 1-2, pp. 207–226, 2013.

[9] H. R. Hao, H. B. Bai, and H. J. Zhang, "Comparison of damping properties between non-circular wire metal rubber and ordinary metal rubber," *Mechanical Science and Technology for Aerospace Engineering*, vol. 28, no. 2, pp. 210–213, 2009.

[10] Y. Y. Li and X. Q. Huang, "Influence parameters of damping properties of metal rubber materials," *Journal Vibration Measurement and Diagnosis*, vol. 29, no. 1, pp. 23–26, 2009.

[11] Y. Wang, B. L. Liu, and Y. R. Lei, "Effect of loading speed on damping characteristics of metal rubber," *Rare Metal Materials and Engineering*, vol. 41, no. 2, pp. 381–383, 2012.

[12] B. Zhu, Y. H. Ma, D. Y. Zhang, and J. Hong, "Study on the constitutive model of hysteresis characteristics of metal rubber," *Journal of Physics*, vol. 61, no. 7, pp. 1–6, 2012.

[13] F. L. Cao, H. B. Bai, and G. Q. Ren, "Constitutive model of metal rubber material based on curved cantilever beam of variable length," *Journal of Mechanical Engineering*, vol. 48, no. 24, pp. 65–70, 2012.

[14] G. P. Zou, Z. Liu, and Z. L. Chang, "Consititutive relation of metal-net rubber," *Aerospace Power Journal*, vol. 31, no. 10, pp. 2318–2324, 2016.

[15] W. Peng, H. B. Bai, and J. Zheng, "Mesoscopic constitutive model of metal rubber material based on combined deformation of micro spring," *Journal of Experimental Mechanics*, vol. 20, no. 3, pp. 455–462, 2005.

[16] Y. Y. Li and X. Q. Huang, "Constitutive relation for metal-rubber with different density and shape factor," *Aerospace Power Journal*, no. 4, pp. 1084–1090, 2008.

[17] H. R. Ao, H. Y. Jiang, S. G. Wang, Y. H. Xia, and A. M. Ulanov, "Research on vibration isolation performance of metal rubber damper supporting engine pipeline," *Journal of Mechanical Design*, no. 2, pp. 14–17, 2003.

[18] Y. Se-Hyun, Y.-S. Jang, and J.-H. Han, "Development of a three-axis hybrid mesh isolator using the pseudoelasticity of a shape memory alloy," *Smart Materials and Structures*, vol. 20, no. 7, article 075017, 2011.

[19] S.-C. Kwon, S.-H. Jeon, and H.-U. Oh, "Performance investigation of a novel pseudoelastic SMA mesh washer gear wheel with micro-jitter attenuation capability," *Smart Materials and Structures*, vol. 25, no. 5, pp. 1–14, 2016.

[20] H.-U. Oh, S.-H. Jeon, T.-H. Kim, and Y.-H. Kim, "Experimental feasibility study for micro-jitter attenuation of stepper-actuated X-band Antenna-pointing mechanism by using pseudoelastic SMA mesh washer," *Smart Materials and Structures*, vol. 24, no. 4, pp. 1–12, 2015.

[21] F. L. Cao, H. B. Bai, and D. W. Li, "Research on mechanical model of metal rubber for hysteresis characteristic in the non-forming direction," *Journal of Mechanical Engineering*, vol. 51, no. 2, pp. 84–89, 2015.

[22] M. Ruo, D. Y. Zhang, and H. X. Zhu, "Finite element simulation method of metal rubber based on tested parameter identification," *Journal of Aeroengine*, vol. 43, no. 3, pp. 56–61, 2017.

[23] R. P. Wu, H. B. Bai, and C. H. Lu, "Analysis of radial compressive properties and mechanical model for ring metal rubber," *Mechanical science and technology for Aerospace Engineering*, vol. 37, no. 4, pp. 635–640, 2018.

[24] Y. Y. Li, X. Q. Huang, and K. Song, "Contacting mechanism of nonlinear friction pair for metallic rubber and its simulation results," *Journal of Vibration And Shock*, vol. 30, no. 7, pp. 77–81, 2011.

[25] J. F. Hou, H. B. Bai, D. W. Li, Y. Y. Wang, and S. Tao, "Experimental study on fatigue properties of metal rubber materials at high and low temperature," *Aerospace Materials and Technology*, no. 2, pp. 77–80, 2007.

[26] S.-C. Kwon, S.-H. Jeon, and H.-U. Oh, "Performance evaluation of spaceborne cryocooler micro-vibration isolation system employing pseudoelastic SMA mesh washer," *Cryogenics*, vol. 67, pp. 19–27, 2015.

[27] H.-U. Oh, S.-C. Kwon, and S.-H. Youn, "Characteristics of spaceborne cooler passive vibration isolator by using a compressed shape memory alloy mesh washer," *Smart Materials and Structures*, vol. 24, no. 1, pp. 1–11, 2015.

[28] S.-C. Kwon, M.-S. Jo, and H.-U. Oh, "Experimental validation of fly-wheel passive launch and on-orbit vibration isolation system by using a superelastic SMA mesh washer isolator," *International Journal of Aerospace Engineering*, vol. 2017, Article ID 5496053, 16 pages, 2017.